Efficient solar photocatalyst based on Ag₃PO₄/graphene nanosheets composite for photocatalytic decolorization of dye pollutants

R. Jiang, H.-Y. Zhu, J.-B. Li, F.-Q. Fu, J. Yao, X.-X. Liang, R.-Q. Guo & G.-M. Zeng

Springer

CrossMark

ORIGINAL PAPER

Efficient solar photocatalyst based on Ag_3PO_4/graphene nanosheets composite for photocatalytic decolorization of dye pollutants

R. Jiang[1,2] · H.-Y. Zhu[1,2] · J.-B. Li[2] · F.-Q. Fu[1] · J. Yao[1] · X.-X. Liang[2] · R.-Q. Guo[3] · G.-M. Zeng[4]

Abstract Silver orthophosphate-graphene nanosheets composite (Ag_3PO_4-GNs) has been fabricated using a facile hydrothermal method. The Ag_3PO_4-GNs were characterized using XRD, UV–vis DRS and SEM. The photocatalytic activity of Ag_3PO_4-GNs was evaluated by photocatalytic decolorization of dye aqueous solutions under simulated solar light irradiation. It was observed that Ag_3PO_4 nanoparticles in Ag_3PO_4-GNs were attached on the surface of graphene nanosheets. The introduction of graphene nanosheets enhanced remarkably the visible light absorption region of Ag_3PO_4-GNs compared with bare Ag_3PO_4. The photocatalytic activity of Ag_3PO_4-GNs is nearly twice as high as that of the pure Ag_3PO_4. The removal efficiency can reach more than 90 % by Ag_3PO_4-GNs under simulated solar light irradiation within 25 min, which might mainly be attributed to high adsorption capacity, extended light absorption range and efficient charge separation. After irradiation for 60 min, 84.70 % TOC mineralization was achieved by Ag_3PO_4-GNs. Based on the results of detection of active species, the direct oxidization of dye pollutants in aqueous solution by holes takes a major role in the whole decolorization process by Ag_3PO_4-GNs. As a result, Ag_3PO_4-GNs with the high photocatalytic activity are proven to be an excellent light photocatalyst for potentially scalable removal of dyes in aqueous solutions and other environmental remediation under simulated solar light irradiation.

Introduction

With rapid industrial developments, a large number of various hazardous pollutants are released into the open environment. Among of those pollutants, toxic organic dyes and their effluents become one of the main sources of water pollution because of the greater demand in textiles, cosmetics and other industries [1, 2]. There are more than 100,000 commercially available dyes with an estimated annual production of over 7×10^5 tons of dye-stuff [3]. Industrial dyeing processes lead to the annual discharge of 30,000–150,000 tons of dyes into receiving waters [4]. Effluents from those industries have high content with organic pollutants, salts, chemical oxygen demand (COD), suspended solids (SS) and fluctuating pH [5]. What's more, dye wastewater contains complex composition, making the conventional biological treatment method restricted. As a result, large amount of scientific and technological efforts have been paid toward for effective treatment of those dye wastewater. Among them, photocatalytic oxidation by photocatalysts is found to be one of the most hopeful and most effective methods to degrade dyes wastewater and get rid of them [6, 7].

✉ H.-Y. Zhu
  zhuhuayue@126.com

✉ G.-M. Zeng
  zgming@hnu.cn
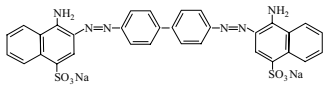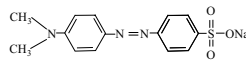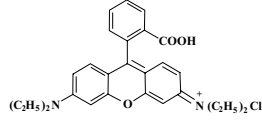
1 Zhejiang Provincial Key Laboratory of Plant Evolutionary Ecology and Conservation, Taizhou University, No.1139, Municipal Government Avenue, Taizhou, Zhejiang 318000, People's Republic of China

2 Environmental Engineering Program, University of Northern British Columbia, Price George, BC V2N 4Z9, Canada

3 College of Physics and Electronic Engineering, Taizhou University, Taizhou 318000, People's Republic of China

4 Key Laboratory of Environmental Biology and Pollution Control (Hunan University), Ministry of Education, Changsha 410082, People's Republic of China

Table 1 Properties of congo red, methyl orange, and Rhodamine B

Dye name	Molecular formula	Molecular weight (g/mol)	CAS number	Molecular structure
Congo red	$C_{32}H_{22}N_6O_6S_2Na_2$	696.68	573-58-0	
Methyl orange	$C_{14}H_{14}O_3N_3SNa$	327.33	547-58-0	
Rhodamine B	$C_{28}H_{31}ClN_2O_3$	479.01	81-88-9	

Very recently, silver orthophosphate (Ag_3PO_4) semiconductor with a band gap of ~2.3 eV exhibits significant photocatalytic decolorization of organic dyes under visible-light irradiation [8, 9]. Therefore, Ag_3PO_4 is one of the most promising photocatalysts in harvesting solar energy for clean energy production and environmental purification [8, 10–13]. To further enhance photocatalytic activity of Ag_3PO_4, different strategies have been developed [14]. Some composites of Ag_3PO_4, such as $SrTiO_3$/Ag_3PO_4 [13], Ag_3PO_4/CNTs [15], Ag_3PO_4/In(OH)$_3$ [16], and PANI/Ag/Ag_3PO_4 [14], have been proven significant enhancement of photocatalytic activity for eliminating dye pollutants. Graphene with 2D carbon nanostructures can potentially serve as a support material with which to anchor semiconductors, and to improve the performance of photoelectronic and energy conversion devices [17]. In particular, outstanding conductive ability (mobility of charge carriers 200,000 cm^2 V^{-1} s^{-1} at room temperature) and an extremely high theoretical specific surface area (theoretically, 2630 m^2/g [18, 19]) can reduce the photo-generated electron–hole (e^-/h^+) recombination rate and improve the photocatalytic properties of photocatalyst [19, 20]. In recent years, graphene has caught immense research attention to synthesize various graphene/semiconductors and investigate its application for environmental remediation and water purification [21–25]. More recently, Ag_3PO_4/graphene composite [11, 26] and Ag_3PO_4/reduced graphene composite [27, 28] have been reported. With the introduction of graphene, the photocatalytic performance and photostability of Ag_3PO_4/graphene were greatly enhanced due to the improved separation efficiency of photogenerated carriers and adsorption performance [11, 26]. However, high price of graphene limits its application for practical water treatment. Graphene nanosheets (GNs) are atomic-thickness monolayers of hexagonally arranged, graphite-derived carbon atoms that may be composed of graphene, graphene oxide, or reduced graphene oxide. They have attracted tremendous interest in their potential application for environmental remediation and water purification [29, 30]. Furthermore, GNs cost only one twentieth of the price of graphene (GNs $15 g^{-1}, graphene $308 g^{-1}). To the best of our knowledge, no previous studies regarding the hydrothermal synthesis and photocatalytic performance of Ag_3PO_4-graphene nanosheets (Ag_3PO_4-GNs) have been reported.

In this study, Ag_3PO_4-GNs have been fabricated via a facile hydrothermal method. The composition, morphology, and optical properties of the as-prepared Ag_3PO_4-GNs were characterized using SEM, XRD and UV–vis DRS. The photocatalytic performance of Ag_3PO_4-GNs was evaluated by the decolorization of three dyes (congo red, methyl orange and rhodamine B) as model pollutants in aqueous solution under simulated solar light irradiation. Moreover, the possible mechanism for dyes decolorization by Ag_3PO_4-GNs is proposed based on the experimental results. Our finding can pave a way to develop economical and highly efficient photocatalysts for the removal of organic pollutants for water purification.

Materals and methods

Chemicals

Graphene nanosheets (GNs, purity >99 %) were purchased from Nanjing Xianfeng Nanomaterial Technology Co., Ltd. Congo red (CR), methyl orange (MO) and rhodamine B (RhB) and used as model dyes were purchased from Yongjia Fine Chemical Factory (Wenzhou, China) (Table 1). Silver nitrate ($AgNO_3$, 99 %), sodium hydrogen

Fig. 1 Schematic representation for the preparation of Ag₃PO₄-GNs
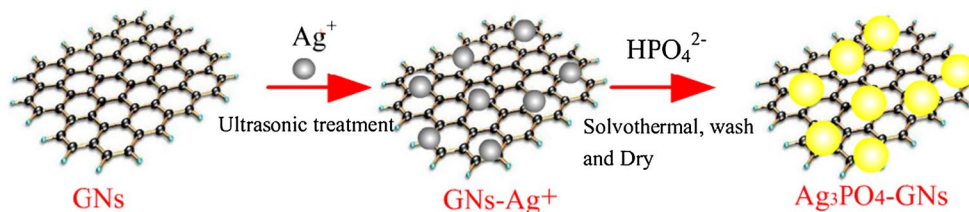
phosphate (Na₂HPO₄, 99 %), edetate disodium salt dehydrate (EDTA-2Na), t-butyl alcohol (TBA), sodium hydrate (99 %) and other reagents of analytical grade were purchased from Shanghai Chemical Reagents Research Institute (Shanghai, China) and were used without further purification.

Preparation of Ag₃PO₄-GNs

Ag₃PO₄-GNs were prepared by a simple hydrothermal method (Fig. 1) [9]. Briefly, silver nitrate was dissolved in 200 mL of double distilled water for 1 h. Fifty grams of GNs were ultrasonically dispersed in the double distilled water (50 mL). The resulted GNs suspension was added into the silver nitrate solution. The suspension system was strongly stirred for 12 h. The positively charged Ag⁺ cations could be assembled onto the surface of the negatively charged GNs [12]. Na₂HPO₄ aqueous solution (0.2 M, 10 mL) was added dropwise to the above system with magnetically stirring. The resulting reaction system was then transferred to a Teflon autoclave and heated at 180 °C for 24 h. After the treatment, the obtained precipitate was collected, washed with double distilled water and ethanol for several times and dried at 100 °C under atmospheric conditions for 10 h until constant weight. The corresponding bare Ag₃PO₄ nanoparticles were also facilely synthesized using the same method but in the absence of GNs.

Characterization of Ag₃PO₄-GNs

X-ray diffraction (XRD) patterns were measured by a Bruker D8 Advance X-ray diffractometer at 40 kV and 50 mA with Cu target and Kα radiation (λ = 0.154178 Å) in the region of 2θ from 10 to 80°. UV–vis diffuse reflectance spectra (DRS) were collected on a Hitachi UV-3100 UV–vis spectrophotometer with BaSO₄ as the background. Scanning electron microscopy (SEM) images were taken using a Hitachi S4800 scanning electron microscope at specific magnification.

Photocatalytic experiments

The photocatalytic experiments of congo red (CR), methyl orange (MO) and rhodamine B (RhB) as model pollutants were carried out in aqueous solutions at ambient

temperature controlled by a watercooling system. A 300 W Xenon lamp (PLS-SXE300, Beijing Trusttech Co. Ltd., China) was used as a simulated solar light source. The wavelength of simulated solar light irradiation was in a range from 300 to 1100 nm. According to a corresponding technical report of PLS-SXE300, UV output (<390 nm) was about 5.2 % of irradiation energy while visible light output (390–770 nm) was about 39.2 %. 0.05 g of photocatalyst was added to 100 mL of simulating pollutant solution contained in a 250 mL Pyrex glass vessel with a plane side. During reaction, the resulting aqueous suspension containing dye and Ag₃PO₄-GNs was continuously stirred and bubbled so that the concentration of dissolved oxygen in the reaction system was kept constant. At given time intervals, about 5 mL aliquots were sampled and centrifuged to remove the photocatalyst. Then concentrations of model pollutants in aqueous solution were determined by a TU 1810 UV–visible spectrophotometer (Beijing Purkinje General Instrument Co., Ltd., China) by monitoring the characteristic absorption wavelength of 553, 463 and 496 nm for RhB, MO and CR, respectively. Decolorization efficiency (η) of dye solution by Ag₃PO₄-GNs at time *t* was calculated by Eq. (1). Total organic carbon (TOC) was measured using a TOC-VCPH analyzer (Shimadzu Co., Japan) to evaluate the mineralization of final dye solutions after the treatments.

$$\eta(\%) = \frac{(C_0 - C_t)}{C_0} \times 100 \tag{1}$$

where C_0 (mg L⁻¹) is the initial dye concentration and C_t (mg L⁻¹) is the dye concentrations at a specific given time *t* (min), respectively.

Results and discussion

Characterization of nanocomposites

Figure 2 shows XRD patterns of graphene nanosheets (GNs), Ag₃PO₄ and Ag₃PO₄-GNs. For GNs, the sharp (0 0 2) diffraction peak of GNs at 2θ = 26.3° was found, suggesting that the characteristic interlayer distance of GNs is about 0.34 nm [31]. Furthermore, the XRD pattern of Ag₃PO₄ clearly show that all distinct diffraction peaks (2θ) at 21.1° (1 1 0), 29.9° (2 0 0), 33.5° (2 1 0), 36.8° (2 1 1),
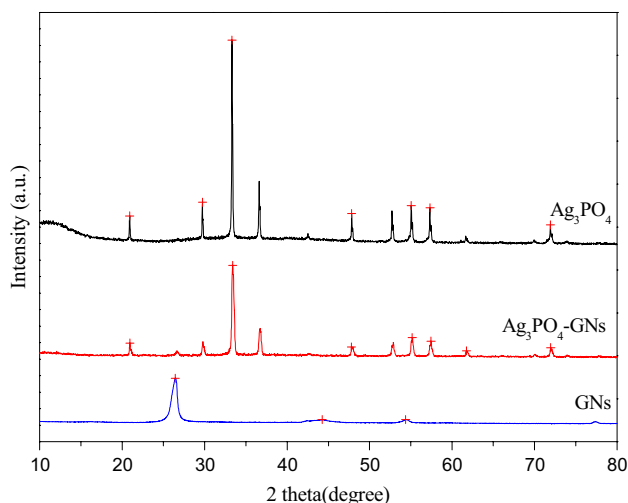
Fig. 2 XRD patterns of GNs, Ag_3PO_4 and Ag_3PO_4-GNs

Fig. 3 UV–vis diffuse reflectance spectra of P25, GNs, Ag_3PO_4 and Ag_3PO_4-GNs

42.7° (2 2 0), 48.0° (3 1 0), 52.9° (2 2 2), 55.2° (3 2 0), 57.5° (3 2 1), 61.8° (4 0 0), 66.0° (3 3 0), 70.1° (4 2 0), 72.1° (4 2 1), 74.0° (3 2 2) could be indexed to the body-centered cubic structure of Ag_3PO_4 (JCPDS no.06-0505), which agrees well with previously reported work [10, 12, 32, 33]. No other characteristic peak was observed, indicating the high purity of the product formed via a facile hydrothermal method. As for Ag_3PO_4-GNs, the above peaks belonging to Ag_3PO_4 nanocrystal can be clearly indexed, and the peak at 25.3° indexed to (0 0 2) plane of GNs can be found. In the range of $2\theta = 10$–80°, no other peaks could be observed, which also confirmed that the composite was exclusively a cubic phase Ag_3PO_4 crystal and GNs [25]. Notably, the diffraction peak at 26.3° belonging to the separate GNs decreased in the Ag_3PO_4-GNs. This results from two facts that the partly disrupted layer-stacking regularity of GNs by the intercalation of Ag_3PO_4 particles and the very low amount of GNs in the Ag_3PO_4-GNs.

UV–vis spectral measurements were employed to measure the changes in the absorption of GNs, Ag_3PO_4, Ag_3PO_4-GNs and P25, as shown in Fig. 3. GNs has exhibited strong absorption ability in both the visible light and UV light ranges, while bare Ag_3PO_4 could absorb solar energy with a wavelength shorter than 530 nm [10]. Compared with the bare Ag_3PO_4, the Ag_3PO_4-GNs display continuous strong absorption in the range of 530–800 nm. A similar result has also been reported on Ag_3PO_4/carbon nanotube composite [34]. This suggests that Ag_3PO_4 particles have been enwrapped by GNs sheets. The possible reason is that the GNs are an excellent light absorptive material and possess a broad absorbance in the visible range. Therefore, as a precondition for effective photodecomposition of organic pollutants, the light absorbing property of Ag_3PO_4-GNs co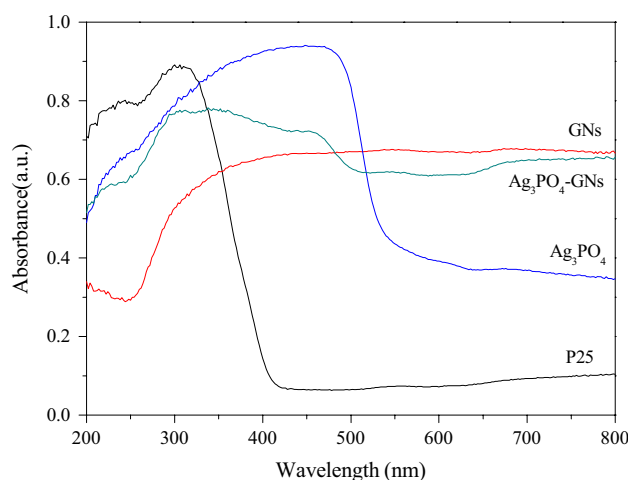mposites has been greatly enhanced. Generally, the wider range of light absorption is beneficial to increase the photocatalytic activity of photocatalysts. As a result, the Ag_3PO_4-GNs composite is suitable to be used for potentially removal of dyes in aqueous solution and other environmental remediation under simulated solar light irradiation.

Figure 4 displays SEM images of GNs, Ag_3PO_4 and Ag_3PO_4-GNs for evaluation of their morphologies. Figure 4a shows the SEM image of GNs before the attachment of Ag_3PO_4. GNs have a crumpled layered structure with thin thickness (5–20 nm) and smooth surface, and wrinkled edge [17]. Ag_3PO_4 exhibited a body-centered cubic structure with grain sizes of 5–20 µm (Fig. 4b), which was accordant with former report. In Fig. 4c, this nanosheet morphology of GNs in Ag_3PO_4-GNs is retained even after the hydrothermal treatment for 24 h at 180 °C. It was observed that Ag_3PO_4 nanoparticles in Ag_3PO_4-GNs were attached on the surface of graphene nanosheets. The size of the Ag_3PO_4 in the Ag_3PO_4-GNs system decreased to 0.5 µm. The size of the Ag_3PO_4-GNs was in micrometer scale both in length and width, which allowed an easy separation from the reaction system by conventional filtration.

Photocatalytic activity

The photocatalytic activity of the as-obtained samples was evaluated by photocatalytic decolorization of CR dye under simulated solar light irradiation, and the results were displayed in Fig. 5. As seen from Fig. 5a, the decolorization efficiency of CR solution can reach 68.3 % by the Ag_3PO_4-GNs after irradiation for 10 min, increased by 24.3 % compareed with the bare Ag_3PO_4. The 10 ppm CR solution was almost completely decolorized by the Ag_3PO_4-GNs within 60 min irradiation. The effective mineralization of organic compounds is very important due to avoiding
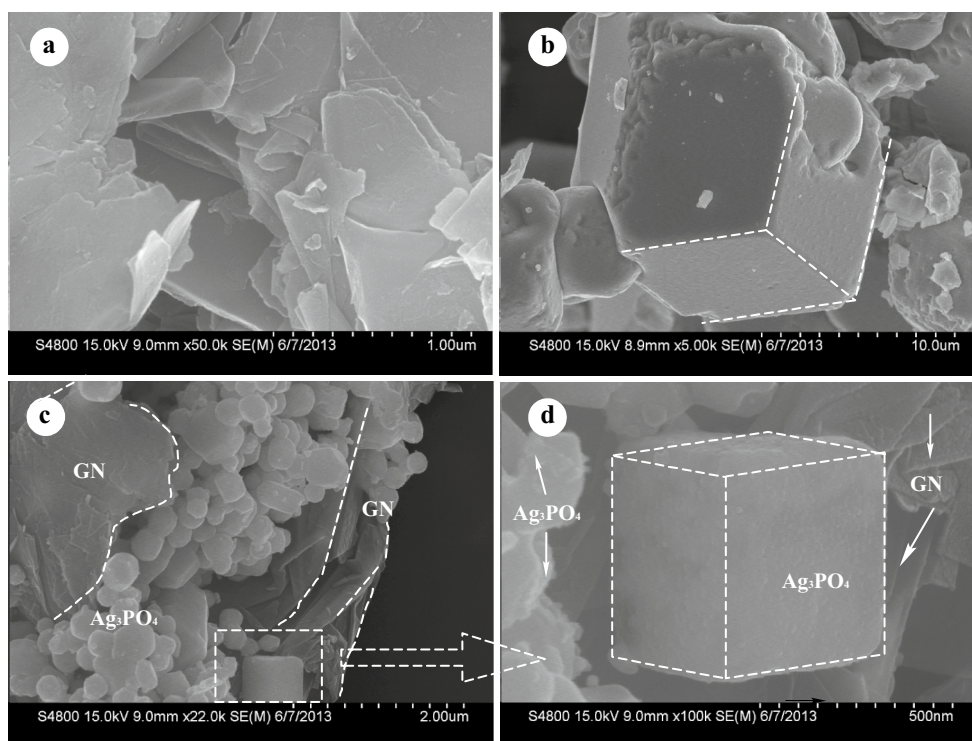
Fig. 4 SEM images of GNs (**a**), Ag$_3$PO$_4$ (**b**) and Ag$_3$PO$_4$-GNs (**c** and **d**)
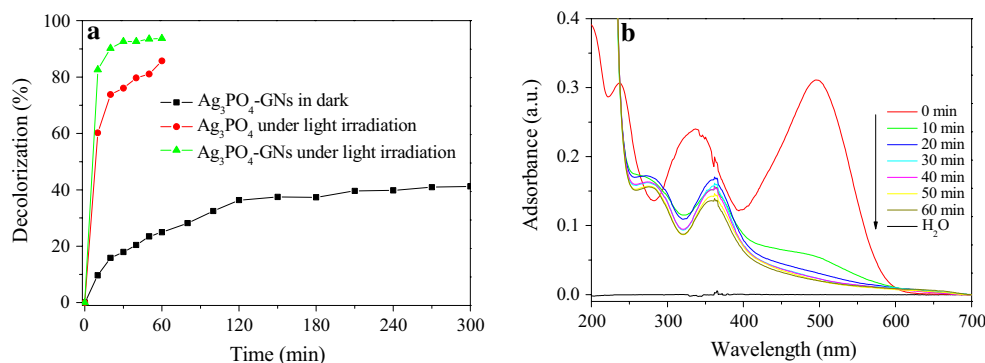

Fig. 5 Comparison of the treatment performances of CR solutions under different conditions (**a**) and UV–vis spectra for decolorization of CR solution under simulated solar light irradiation on Ag$_3$PO$_4$-GNs (**b**)

secondary pollution in the practical application of photocatalytic technology. In this system, total organic carbon (TOC) was chosen as a mineralization index. After irradiation for 60 min, 84.70 % TOC mineralization was achieved by Ag$_3$PO$_4$-GNs under simulated solar light irradiation. Obviously, the addition of an appropriate amount of GNs could enhance the photoactivity effectively. The photocatalytic decolorization of CR solution over the photocatalysts matches the pseudo-first-order kinetics by linear transform $\ln(C_0/C_t) = kt$. The initial apparent rate constant k over Ag$_3$PO$_4$-GNs is 0.1277 min^{-1}, which is nearly two times

as high as that of the pure Ag$_3$PO$_4$. Figure 5b shows the temporal evolution of the spectral changes of CR dye solution mediated by Ag$_3$PO$_4$-GNs. As observed from Fig. 5b, absorption spectrum of the original CR solution was characterized by two main bands at 496 and 338 nm. The absorbance peak at 496 nm was attributed to the azo bonds of CR molecule while the absorbance peak at 338 nm was attributed to "benzene, naphthalene rings" structures. During photocatalysis of CR solution by Ag$_3$PO$_4$-GNs, the absorption peak of CR solution at 496 nm decreased gradually and disappeared finally, which is in accordance with
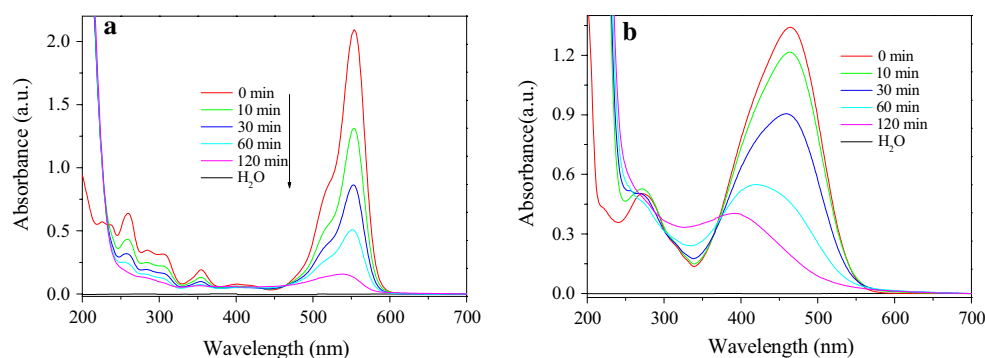
Fig. 6 Time-dependent UV–vis spectra of degraded RhB solution (**a**) and MO solution (**b**) photocatalyzed by Ag$_3$PO$_4$-GNs

the color change from red to colorlessness of the CR solution with increasing irradiation time. According to the previous report, the azo groups of CR were removed, and then the cycloreversion occurred during the decolorization of CR solution [7]. To clarify whether the adsorption behavior by photocatalysts is responsible for the decolorization of CR solution, the efficiency of adsorption is determined by measuring the evolution of CR dye concentration. The adsorption efficiency of CR by Ag$_3$PO$_4$-GNs is two times higher than that of bare Ag$_3$PO$_4$. The carbon in GNs plays important roles during the photocolorization of dye solution by increasing adsorption capacity of Ag$_3$PO$_4$-GNs. High and fast adsorption of CR on Ag$_3$PO$_4$-GNs can be attributed to the strong interaction from the π–π stacking between aromatic regions of GNs and dye molecular [24], which is profitable for the succedent photocatalytion of CR solution. As a result, the enhanced photocatalytic activity of Ag$_3$PO$_4$-GNs might be attributed to high adsorption capacity of dyes, extended light absorption range and efficient charge separation due to giant π-conjugation system and two-dimensional planar structure of GNs in Ag$_3$PO$_4$-GNs.

Furthermore, two other dyes (MO and RhB) were also chosen to evaluate the photocatalytic activity of Ag$_3$PO$_4$-GNs. All the experimental conditions were the same as those of CR decolorization. From the temporal evolution of the spectral changes of MO and RhB solutions mediated by Ag$_3$PO$_4$-GNs under visible light irradiation (Fig. 6a, b), the absorbance spectral lines clearly indicates the gradual, significant and steady decrease in both the absorbance of MO and RhB dyes. The percentage decolorization of MO and RhB at the maximal absorption wavelength was accounted to be 71 and 85 %, respectively, by the end of 120 min of exposure.

The proposed photocatalytic mechanism

Generally, the elimination of organic compounds in aqueous solution by photocatalysis can be attributed to both the
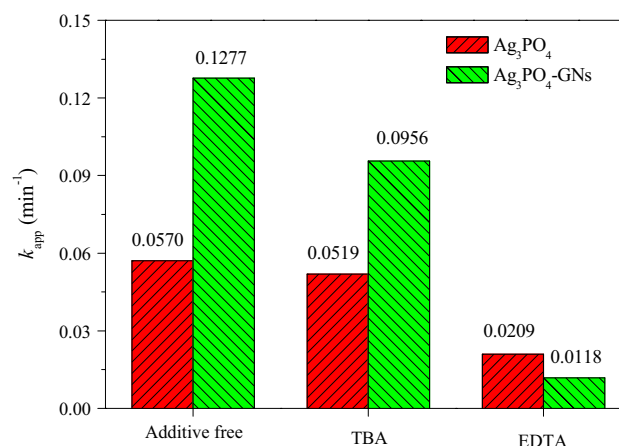

Fig. 7 Effects of hydroxyl radical and hole scavengers on the decolorization rate of CR dye photocatalyzed by Ag$_3$PO$_4$-GNs composite and Ag$_3$PO$_4$

adsorption and oxidation properties of reactive species, such as h^+ and •OH [35]. To investigate the photocatalytic mechanism of the Ag$_3$PO$_4$-GNs in more detail, different specific scavengers were used to determinate the influences of •OH and h^+ on the decolorization rates of CR. In this study, t-butyl alcohol (TBA) and edetate disodium salt dehydrate (EDTA-2Na), acted as the scavengers for •OH and h^+ [36], were introduced into the photocatalytic process, respectively. Figure 7 shows the corresponding pseudo-first-order rate constants of CR dye over Ag$_3$PO$_4$ and Ag$_3$PO$_4$-GNs with and without scavengers under simulated solar light irradiation.

At first, the rate constant of CR decolorization by Ag$_3$PO$_4$-GNs composite was 0.1277 min^{-1}, which was about twice as high as that of pure Ag$_3$PO$_4$ (0.0570 min^{-1}). This revealed that the photocatalytic ability of Ag$_3$PO$_4$-GNs composite was higher than that of pure Ag$_3$PO$_4$. For Ag$_3$PO$_4$, the photocatalytic decolorization rate constant was obtained as 0.0570 min^{-1} without scavengers, but it

Fig. 8 Schematic of proposed mechanism of photocatalysis decolorization of dye by Ag_3PO_4-GNs
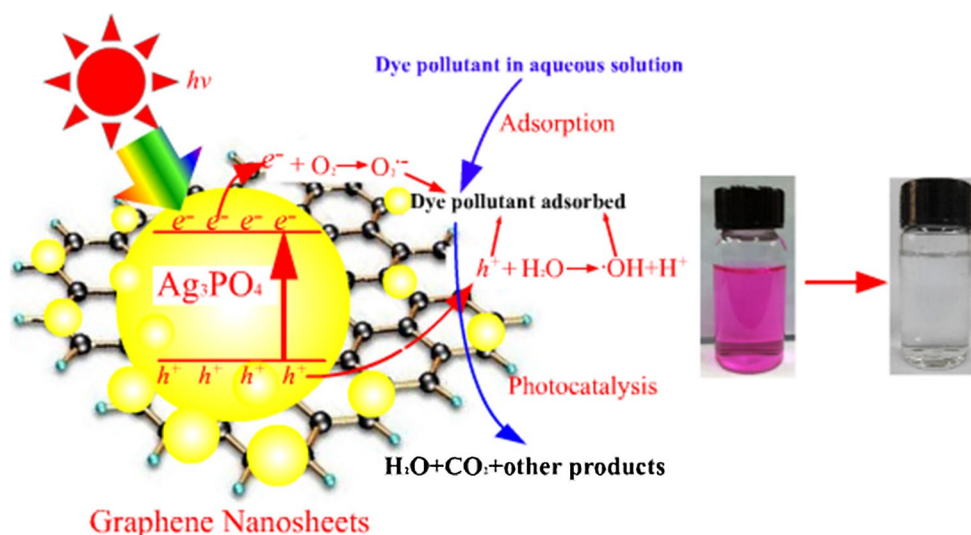
decreased to 0.0519 and 0.0209 min^{-1} with the addition of TBA or EDTA-2Na, respectively, demonstrating the contribution of •OH and h^+ with 8.9 and 53.9 %, respectively. As shown in Fig. 7, the addition of TBA almost did not affect the decolorization rate of CR solution by Ag_3PO_4, suggesting that •OH was of less importance in the photocatalytic process. However, the decolorization percence of CR solution was still on in the presence of EDTA-2Na under simulated solar light irradiation, indicating some other reactive species besides holes (h^+) were involved, such as •HO_2, •O_2^-, and so on. In fact, some previous studies have reported that the photogenerated holes of Ag_3PO_4 cannot oxidize OH^-/H_2O to form •OH due to their little difference of potentials [37].

However, for Ag_3PO_4-GNs, the photocatalytic decolorization rate constant decreased from 0.1277 to 0.0956 min^{-1} and 0.0118 min^{-1} with the addition of TBA or EDTA, respectively. With the introduction of GNs to Ag_3PO_4, the photocatalytic decolorization of CR solution was obviously suppressed after the addition of TBA. When EDTA (hole scavengers) was added into the photocatalytic system, a notable inhibitory effect on the decolorization activity over the Ag_3PO_4-GNs composite was observed, in which less than 10 % rates constant were kept. The same result was also reported by Yang [38]. As is well known, an efficient charge separation/transfer is crucial for the enhancement of photocatalytic activities. The transfer of the holes from valence band (VB) of Ag_3PO_4-GNs was accelerated with the addition of GNs. In fact, GNs could act as a support and electron acceptor to suppress the charge recombination of Ag_3PO_4 and enhance the photocatalytic activity and stability of Ag_3PO_4 [9, 17, 39]. It can be concluded that the direct oxidization of pollutants by holes takes a major role in the whole decolorization process by Ag_3PO_4-GNs under

simulated solar light irradiation. The high reactive •OH formed in the photocatalytic system was found to be other major responsible for the photocatalytic decolorization of dye solution by for Ag_3PO_4-GNs.

Based on the results of the addition of active species scavengers, the possible mechanism for photocatalytic decolorization of organic dyes by Ag_3PO_4-GNs was proposed and represented in Fig. 8. At first, the objective dye molecular in aqueous solution was adsorbed on the surface of Ag_3PO_4-GNs by the strong interaction from the π–π stacking between aromatic regions of GNs and dye molecules [40]. It would be easier for the photo-generated active species to oxidize the surface adsorbed dye pollutants. At the same time, the activated Ag_3PO_4 in Ag_3PO_4-GNs generated electron–hole (e^-/h^+) pairs in the conduction band (CB) and the valence band (VB) under simulated solar light irradiation, respectively [8]. The excited e^- of photocatalyst could transfer from the conduction band to GNs via a percolation mechanism in GNs-photocatalyst [41, 42] since GNs have been reported to be a competitive candidate for the acceptor material due to its two dimensional π-conjugation structure. During photocatalytic reaction, the aqueous suspension containing both objective dye pollutants and Ag_3PO_4-GNs was continuously stirred and bubbled. As a result, the transfer e^- are scavenged by the dissolved molecular oxygen in dye solution or the adsorbed molecular oxygen on the Ag_3PO_4-GNs surface to produce superoxide anion ($O_2^{\bullet-}$) radicals. The photogenerated h^+ on VB of Ag_3PO_4 partly oxidize water to form hydroxyl radicals (•OH). At last, together with •OH and $O_2^{\bullet-}$, the resultant h^+ in the VB of Ag_3PO_4 in Ag_3PO_4-GNs could undergo chain reactions to degrade and mineralize partially or completely organic dye pollutant in aqueous solution [43].

Conclusions

In conclusion, Ag_3PO_4-graphene nanosheets composite (Ag_3PO_4-GNs) with high performance has been fabricated via a facile hydrothermal method. Ag_3PO_4-GNs possessed a wide and extended spectral response, and enhanced charge separation and transportation properties simultaneously. Ag_3PO_4-GNs exhibited excellent photocatalytic activity in decolorization of three model contaminants including congo red, methyl orange and Rhodamine B. The enhanced photocatalytic activity of the composite catalysts might be attributed to high adsorption capacity of dyes, extended light absorption range and efficient charge separation due to giant p-conjugation system and two-dimensional planar structure of graphene. Based on the results of detection of active species, it can be concluded that the direct oxidization of pollutants by holes takes a major role in the whole decolorization process by Ag_3PO_4-GNs under simulated solar light irradiation. Due to the high activity of Ag_3PO_4-GNs composites, it probably has potential applications for environmental remediation and water purification under simulated solar light irradiation.

References

1. M. Ghaemi, G. Absalan, L. Sheikhian, J. Iran. Chem. Soc. **11**, 1759 (2014)
2. M. Azadi, A. Habibi-Yangjeh, J. Iran. Chem. Soc. **12**, 909 (2015)
3. E. Brillasa, C.A. Martínez-Huitle, Appl. Catal. **B 166–167**, 603 (2015)
4. K. Yu, S. Yang, C. Liu, H. Chen, H. Li, C. Sun, S.A. Boyd, Environ. Sci. Technol. **46**, 7318 (2014)
5. Y. Xiong, P.J. Strunk, H.Y. Xia, X.H. Zhu, H.T. Karlsson, Water Res. **35**, 4226 (2001)
6. F.N. Chianeh, J.B. Parsa, J. Iran. Chem. Soc. **12**, 175 (2015)
7. H.Y. Zhu, R. Jiang, L. Xiao, Y.H. Chang, Y.J. Guan, X.D. Li, G.M. Zeng, J. Hazard. Mater. **169**, 933 (2009)
8. Z. Yi, J. Ye, N. Kikugawa, T. Kako, S. Ouyang, H. Stuart-Williams, H. Yang, J. Cao, W. Luo, Z. Li, Y. Liu, R. Withers, Nat. Mater. **9**, 559 (2010)
9. L. Liu, J. Liu, D.D. Sun, Catal, Sci. Technol. **2**, 2525 (2012)
10. Y. Bi, S. Ouyang, N. Umezawa, J. Cao, J. Ye, J. Am. Chem. Soc. **133**, 6490 (2011)
11. G. Chen, M. Sun, Q. Wei, Y. Zhang, B. Zhu, B. Du, J. Hazard. Mater. **244–245**, 86 (2013)
12. H. Cui, X. Yang, Q. Gao, H. Liu, Y. Li, H. Tang, R. Zhang, J. Qin, X. Yan, Mater. Lett. **93**, 28 (2013)
13. X. Guan, L. Guo, ACS Catal. **4**, 3020 (2014)
14. Y. Bu, Z. Chen, ACS Appl. Mater. Interfaces **6**, 17589 (2014)
15. W. Zhai, G. Li, P. Yu, L. Yang, L. Mao, J. Phys. Chem. **C 117**, 15183 (2013)
16. J. Guo, S. Ouyang, H. Zhou, T. Kako, J. Ye, J. Phys. Chem. **C 117**, 17716 (2013)
17. A.A. Ismail, R.A. Geioushy, H. Bouzid, S.A. Al-Sayari, A. Al-Hajry, D.W. Bahnemann, Appl. Catal. **B 129**, 62 (2013)
18. M.D. Stoller, S. Park, Y. Zhu, J. An, R.S. Ruo, Nano Lett. **8**, 3498 (2008)
19. S. Bahar, F. Karami, J. Iran. Chem. Soc. **12**, 2213 (2015)
20. D.R. Dreyer, S. Park, C.W. Bielawski, R.S. Ruoff, Chem. Soc. Rev. **39**, 228 (2010)
21. A. Aghigh, V. Alizdeh, H.Y. Wong, M.S. Islam, N. Amin, M. Zamn, Desalination **365**, 389 (2015)
22. T. Xiong, F. Dong, Y. Zhou, M. Fu, W.K. Ho, J. Colloid Interface Sci. **447**, 16 (2015)
23. N. Zhang, M.Q. Yang, Z.R. Tang, Y.J. Xu, J. Catal. **303**, 60 (2013)
24. K. Li, J. Xiong, T. Chen, L. Yan, Y. Dai, D. Song, Y. Lv, Z. Zeng, J. Hazard. Mater. **250–251**, 19 (2013)
25. Q. Xiang, D. Lang, T. Shen, F. Liu, Appl. Catal. **B 162**, 196 (2015)
26. Y. Ao, P. Wang, C. Wang, J. Hou, J. Qian, Appl. Surface Sci. **271**, 265 (2013)
27. B. Chai, J. Li, Q. Xu, Ind. Eng. Chem. Res. **53**, 8744 (2014)
28. P.Y. Dong, Y.H. Wang, B.C. Cao, S.Y. Xin, L.N. Guo, J. Zhang, F.H. Li, Appl. Catal. **B 132–133**, 45 (2013)
29. Q. Li, B. Guo, J. Yu, J. Ran, B. Zhang, H. Yan, J.R. Gong, J. Am. Chem. Soc. **133**, 10878 (2011)
30. N. Yang, Y. Zhang, J.E. Halpert, J. Zhai, D. Wang, L. Jiang, Small **81**, 762 (2012)
31. T. Peng, K. Li, P. Zeng, Q. Zhang, X. Zhang, J. Phys. Chem. **C 116**, 22720 (2012)
32. J.D. Wang, J.K. Liu, C.X. Luo, Y. Lu, X.H. Yang, Cryst. Growth Des. **13**, 4837 (2013)
33. X. Wang, S. Yuan, S. Chen, G. Chen, J. Zhang, L. Zhang, Res. Chem. Intermed. (2014). doi:10.1007/s11164-014-1617-6
34. Z. Wang, L. Yin, M. Zhang, G. Zhou, H. Fei, H. Shi, H. Dai, J. Mater. Sci. **49**, 1585 (2014)
35. T. An, J. An, Y. Gao, G. Li, H. Fang, W. Song, Appl. Catal. **B 164**, 279 (2015)
36. Y. Liu, W. Yao, D. Liu, R. Zong, M. Zhang, X. Ma, Y. Zhu, Appl. Catal. **B 163**, 547 (2015)
37. Q. Xiang, J. Yu, M. Jaroniec, Chem. Soc. Rev. **41**, 782 (2012)
38. X. Yang, J. Qin, Y. Jiang, K. Chen, X. Yan, D. Zhang, R. Li, H. Tang, Appl. Catal. **B 166–167**, 231 (2015)
39. Y.L. Min, G.Q. He, R.B. Li, W. Zhao, Y.C. Chen, Y.G. Zhang, Sep. Purif. Technol. **106**, 97 (2013)
40. X. Li, T. Zhang, S. Gu, S.Z. Kang, G. Lib, J. Mu, Sep. Purif. Technol. **108**, 139 (2013)
41. X. Wang, L.J. Zhi, K. Mullen, Nano Lett. **8**, 323 (2008)
42. H. Zhang, X. Lv, Y. Li, Y. Wang, J. Li, ACS Nano **4**, 380 (2010)
43. M. Cao, P. Wang, Y. Ao, C. Wang, J. Hou, J. Qian, Int. J. Hydrogen Energy **40**, 1016 (2015)